Integrated Converter Utilizing Tapped-Inductor with Arbitrary Voltage Step-Up Ratio to Enhance Energy Yield for Curved Solar Roofs of PHEVs

Takumi Suzuki
Department of Electrical and Electronic Engineering
Ibaraki University
Ibaraki, Japan
20nm630h@vc.ibaraki.ac.jp

Yusuke Sasaki
Department of Electrical and Electronic Engineering
Ibaraki University
Ibaraki, Japan
19nm630r@vc.ibaraki.ac.jp

Masatoshi Uno
Department of Electrical and Electronic Engineering
Ibaraki University
Ibaraki, Japan
masatoshi.uno.ee@vc.ibaraki.ac.jp

***Abstract*—The characteristic mismatch of photovoltaic (PV) substrings in solar roofs of PHEVs not only triggers a significant reduction in power generation but also malfunctions of maximum power point (MPP) tracking due to the occurrence of multiple MPPs. Differential power processing (DPP) converters based on a switched capacitor converter have been proposed to prevent negative influences of characteristic mismatch. However, a step-up converter is separately required to control panel voltage in addition to a DPP converter, resulting in the increased complexity of PV systems. This paper proposes an integrated converter that realizes system simplification by integrating a PWM step-up converter and a DPP converter. The step-up conversion ratio of the proposed integrated converter can arbitrarily adjust thanks to a tapped inductor. Experiments using a 200-W prototype for seven-substring solar roofs were performed emulating mismatched irradiance conditions, and the results demonstrated the step-up power conversion capability and enhanced power yield.**

Keywords*— *Differential power processing converter, photovoltaic panel, PWM step-up converter, switched capacitor converter, tapped-inductor

I. INTRODUCTION

Plug-in hybrid electric vehicles (PHEVs) with a solar roof, which is a photovoltaic (PV) panels mounted on a PHEV's roof, have been developed and commercialized by various automobile manufacturers. Solar roofs are used to charge auxiliary batteries for electrical equipment, such as ventilation, stereos, and navigation systems.

In general, standard rigid PV panels consist of two or three substrings connected in series. Solar roofs for PHEVs (e.g., Prius PHV), on the other hand, comprise seven substrings, as shown in Fig. 1(a). The curved surface of the solar roof makes its irradiation levels uneven, as illustrated in Fig. 1(b). Therefore, substring characteristics are always mismatched due to the uneven irradiance, as shown in Fig. 2(a). Since the substrings are connected in series and share the same current,

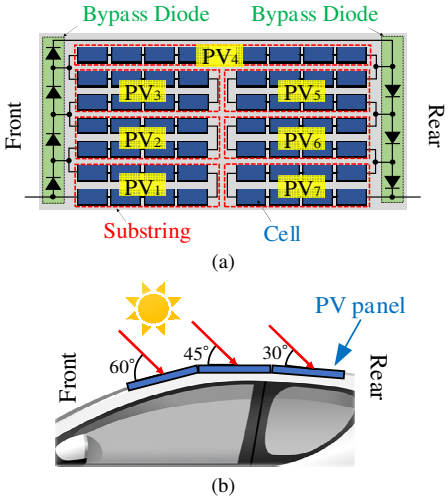

Fig. 1. (a) Configuration of solar roof, (b) PHEV equipped with solar roof.

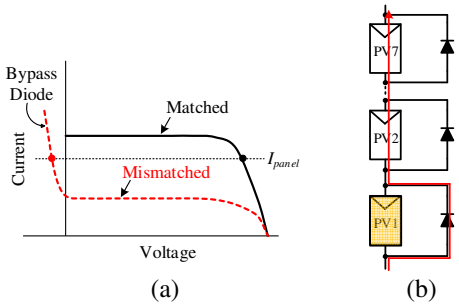

Fig. 2. (a) Substring characteristics under uneven irradiance, (b) current flow when PV1 is weak substring.

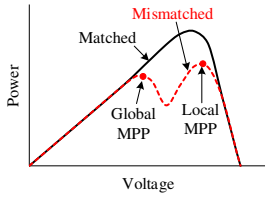

Fig. 3. Panel characteristics under mismatch and partial shading conditions.

some weak substrings with low irradiance are likely bypassed, as shown in Fig. 2(b). Very similar situations are known to happen under so-called partial shading conditions [1]. Since the bypassed substrings no longer contribute to power generation, power yield from the PV panel is significantly reduced, as shown in Fig. 3. In addition, mismatched panel characteristics exhibit multiple maximum power points (MPPs), including a global MPP and local MPP(s). The occurrence of multiple MPPs confuses and hinders the conventional MPP tracking (MPPT) algorithms because the PV panel might operate at a local MPP that is a suboptimal point producing less power than a global MPP [2], [3].

To overcome these issues, cascaded converters [4], dc optimizers [5], microinverters [6], and micro converters [7] have been employed. These converters control all substrings individually. Fig. 4(a) describes a micro dc-dc converter system as a typical example. This system achieves individual MPPT and increases the power yield. However, this system requires as many converters as substrings, and therefore the PV system becomes costly and complicated.

Differential power processing (DPP) converters have been proposed as a powerful alternative solution to the characteristic mismatch issues. Various kind of DPP converters have been proposed, such as bidirectional converters [8], [9], isolated bidirectional converters-based [10]–[12], multistage choppers [13], single-input multi-output converters [14]–[19], switched capacitor converters (SCCs) [20]–[22], etc. DPP converters are connected in parallel with the PV panel to distribute a fraction of the generated power to the weak substrings. This power redistribution virtually unifies all substring characteristics.

DPP converters based on SCCs can be roughly categorized into two groups, so-called ladder SCCs [20] and Dickson SCCs [21], as shown in Figs. 4(b) and 4(c), respectively. The ladder SCCs transfer the power only between adjacent substrings. For example, when transferring the power from PV4 to PV1, multiple power conversion stages are necessary to unify the substrings voltage. The system efficiency decreases due to cumulative loss. By contrast, the Dickson SCCs directly transfer the power to the weak substring. When transferring the power from PV4 to PV1, the power travels via only capacitor C_4 and C_1. This system can reduce the number of power conversion stages. The Dickson SCCs can decrease the cumulative loss and improve the overall efficiency compared with the ladder SCCs in PHEV applications.

PV systems in PHEV applications require a step-up converter not only for boosting the panel voltage to a desired load voltage but also for tracking the MPP of the panel. Fig 5(a) shows the conventional PV systems. In addition to the DPP converter, the step-up converter is separately required, resulting in conventional PV systems are prone to complexity and costly.

To cope with the aforementioned issues, integrated PV systems have been proposed [23], as shown in Fig. 5(b). These systems realize system- and circuit-level simplifications. However, the conventional integrated converter based on the Dickson SCC and the PWM step-up converter has issues that voltage step-up ratio decreases due to the increase in the number of substrings [23].

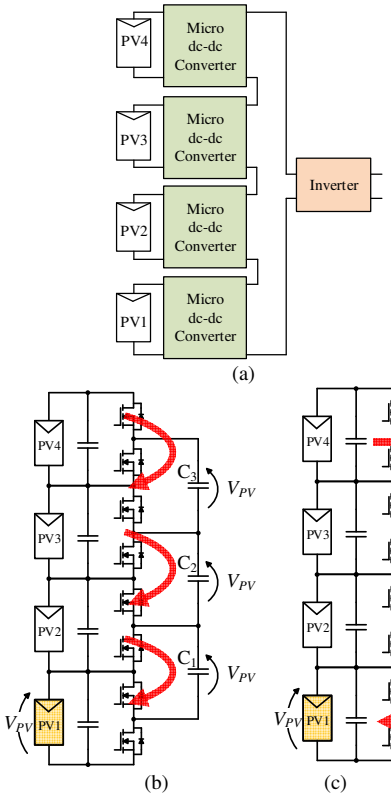

Fig. 4. Solutions to mismatch issues: (a) Micro dc-dc converter, (b) ladder SCC, (c) Dickson SCC.

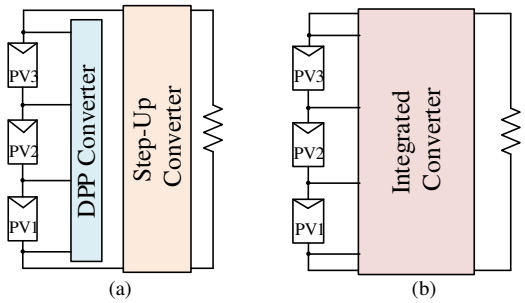

Fig. 5. PV systems for PHEV applications: (a) conventional PV systems, (b) integrated PV systems.

This paper proposes a novel integrated converter based on the Dickson SCC and the PWM step-up converter. The proposed converter can achieve the arbitrary voltage step-up ratio adopting a Tapped-Inductor (TI). The remainders of this paper are as follows. The proposed converter is presented, and the configuration and features are given in Section II. Section III analyses the operation of the proposed converter, and describing the derivation of voltage step-up ratio. The experimental equalization tests using a 200-W prototype presents in Section IV. Conclusions are drawn in Section V.

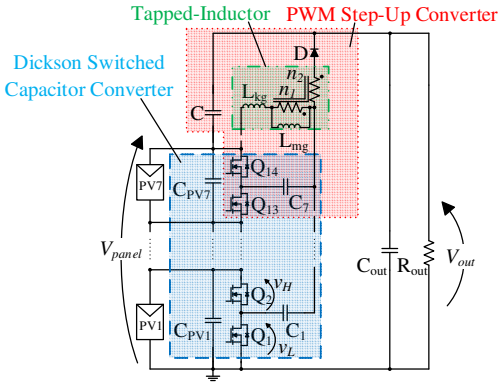

Fig. 6. Proposed converter for seven substrings.

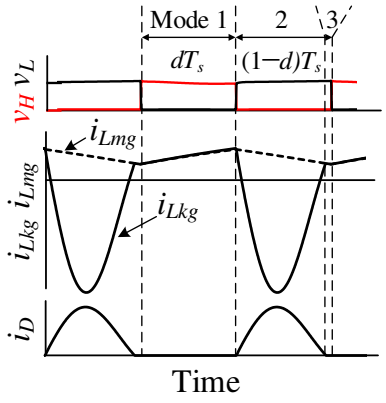

Fig. 7. Theoretical key operation waveforms.

II. Proposed Converter

A. Circuit Configuration

The proposed converter for seven substrings connected in series is shown in Fig. 6. The proposed converter is derived from the integration of the conventional DPP converter based on the Dickson SCC [6] and a PWM step-up converter containing a TI. The SCC comprises the smoothing capacitors C_{PV1}–C_{PV7}, the coupling capacitors C_1–C_7, and switches Q_1–Q_{14}. The PWM step-up converter comprises Q_{13}–Q_{14}, TI, diode D, and the output capacitor C. The TI's winding connected to Q_{14} is defined as the primary side, and the opposite side is defined as the secondary side.

B. Features

The Dickson SCC and the PWM step-up converter are integrated into a single unit with sharing Q_{13} and Q_{14}, realizing system- and circuit-level simplifications by reducing the total switch count. The Dickson SCC not only prevents the characteristic mismatch issues but also reduces the cumulative loss by directly distributing a fraction of the generated power to the weak substrings, as mentioned in Section I. The proposed converter achieves arbitrary step-up voltage conversion ratios by adjusting the turns ratio ($N = n_2/n_1$) of the TI. The theoretical voltage step-up ratio will be derived in Section III-C.

III. Operation Analysis

A. Operation Modes

The principle of the proposed converter does not change with or without characteristic mismatch, and therefore the operation analysis is performed of uniform irradiance condition (i.e., uniform substring characteristic). Dead-time periods are neglected, and all circuit components are assumed ideal. The theoretical key operation waveforms and current flow directions are shown in Figs. 7 and 8, respectively.

Mode 1 [Fig. 8(a)]: The odd- and even-numbered switches are on and off, respectively. The voltage of substring PV1, V_{PV1}, can be expressed as

$$V_{PV1} = V_{C1} - V_{C2} \tag{1}$$

where V_{C1} and V_{C2} are the voltages of C_1 and C_2. The voltage of the magnetizing inductance L_{mg} of the TI, v_{Lmg}, is

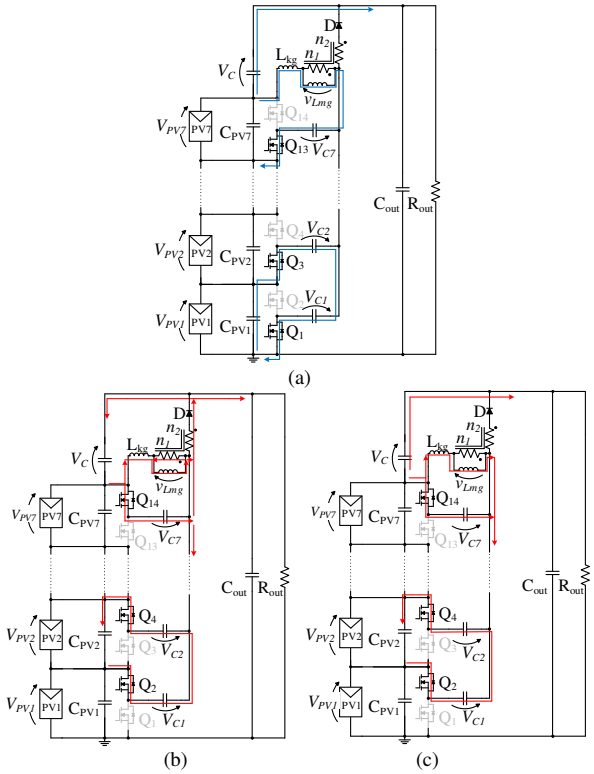

Fig. 8. Current flow directions in (a) Mode 1, (b) Mode 2, and (c) Mode 3.

$$v_{Lmg} = V_{PV7} - V_{C7} \tag{2}$$

where V_{PV7} is the voltage of PV7, and V_{C7} is the voltage of C_7. The current of L_{mg}, i_{Lmg}, linearly increases, and the TI stores energy. The current of the leakage inductance L_{kg}, i_{Lkg}, and i_{Lmg} are the same.

Mode 2 [Fig. 8(b)]: The odd- and even-numbered switches are turned off and on, respectively. The voltage of PV2, V_{PV2}, is equal to the sum voltage of V_{C1} and V_{C2}. V_{PV2} can be represented as

$$V_{PV2} = V_{C1} - V_{C2} \tag{3}$$

From (1) and (3),

$$V_{PV1} = V_{PV2} \tag{4}$$

By the same principle as in the case of PV1 and PV2, the voltage of all substrings becomes the same value.

$$V_{PV1} = V_{PV2} = \cdots = V_{PV7} \tag{5}$$

Since L_{mg} and C_7 are connected in parallel, v_{Lmg} is given by

$$v_{Lmg} = -V_{C7} \tag{6}$$

i_{Lmg} linearly decreases because the voltage polarity of v_{Lmg} is reversed. i_{Lkg} sinusoidally changes due to the resonance between L_{kg} and C_1–C_7. An ac current is transferred to the secondary side of TI, and the current is supplied to the PV7. The voltage of the secondary side of TI is N times as much as the primary ones.

Mode 3 [Fig. 8(c)]: Both i_{Lkg} and i_{Lmg} linearly decrease at the same rate, while no current flows on the secondary side of the TI. Continuing from Mode 2, current flow directions do not change in the Dickson SCC. Turning on and off the odd- and even-numbered switches, respectively brings the operation back to Mode 1.

In summary, all substring voltages become uniform by alternately driving the odd- and even-numbered switches. Consequently, the proposed converter precludes the issues caused by the characteristic mismatch.

B. Relationship between Switching and Resonant Frequency

Half the resonant period must be shorter than the $(1-d)T_s$, where T_s is the switching period and d is the duty cycle of the odd-numbered switches, to operate the proposed converter independently of d, as shown in Fig. 7. The switching frequency f_s and the resonant frequency f_r have to satisfy within the following equation.

$$f_s \le 2(1-d)f_r = \frac{1-d}{\pi\sqrt{L_{kg}\sum_{i=1}^{7} C_i}} \tag{7}$$

C. Derivation of Voltage Step-Up Ratio

The theoretical voltage step-up ratio is obtained from the volt-sec balance on L_{mg}. From (2) and (6), the volt-sec balance is expressed as

$$d(V_{PV7} - V_{C7}) + (1-d)(-V_{C7}) = 0 \tag{8}$$

Therefore, V_{C7} can be obtained:

$$V_{C7} = dV_{PV7} \tag{9}$$

As shown in Fig. 8(b), C is charged via D by the series connection of C_7 and the secondary winding of TI. Because the voltage of the secondary side of TI is NV_{C7}, the voltage of C, V_C, can be expressed as

$$V_C = NV_{C7} + V_{C7} \tag{10}$$

Substituting (9) into (10) produces

$$V_C = d(1+N)V_{PV7} \tag{11}$$

The voltage of all substrings is assumed the same by the operation of the Dickson SCC, the panel voltage V_{panel} is

$$V_{panel} = 7V_{PV7} \tag{12}$$

From (11) and (12), V_C can be expressed as

$$V_C = \frac{d(1+N)V_{panel}}{7} \tag{13}$$

The sum voltage of V_{panel} and V_C is equal to the output voltage, V_{out}, as

$$V_{panel} + V_C = V_{out} \tag{14}$$

By substituting (13) into (14), the theoretical voltage step-up ratio can be obtained:

$$\frac{V_{out}}{V_{panel}} = 1 + \frac{d(1+N)}{7} \tag{15}$$

Fig. 9 shows theoretical and simulated voltage step-up ratios as a function of d. The simulation characteristics show the good agreement with the theoretical ones. The result demonstrates that the voltage step-up ratio of the proposed converter can arbitrarily adjust thanks to a TI.

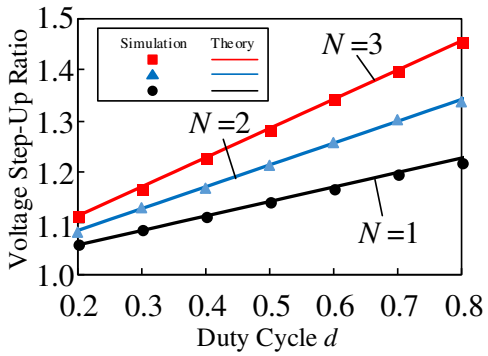

Fig. 9. Theoretical and simulated voltage step-up ratios as a function of duty cycle d.

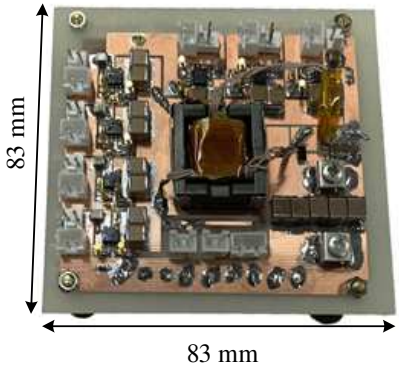

Fig. 10. 200-W prototype for seven substrings.

TABLE I. COMPONENT VALUES.

Component	Value
C_{PV1}–C_{PV7}	Ceramic Capacitor, 220 μF
C_1–C_7	Ceramic Capacitor, 15 μF×2
C_{out}	Ceramic Capacitor, 22 μF×4
C	Ceramic Capacitor, 100 μF×3
D	Schottky Barrier Diode V_f = 0.44 V
Tapped-Inductor	n_1:n_2 = 1:2.83 L_{kg} = 0.22 μH, L_{mg} = 29.4 μH
MOSFET	FDS6990A $R_{DS(ON)}$ = 31 mΩ
Gate Driver	UCC27201D

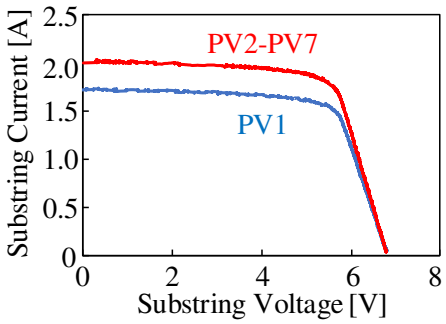

Fig. 11. Individual substring characteristics.

IV. EXPERIMENTAL RESULTS

A. Prototype

A 200-W prototype of the proposed converter for seven substrings connected in series was built, as shown in Fig. 10. Component values are listed in Table I. *N* of TI was designed to be 2.83 to operate at $d = 0.5$ when the MPP-voltage of the panel was 38 V and the output voltage was 48 V.

B. Experimental Equalization Tests Emulating Mismatched Irradiance Condition

An experimental equalization test using solar array simulators (Keysight Technologies, E4360A) was performed, emulating the mismatched condition where PV1 only was mismatched. Individual substring characteristics used for the experiment are shown in Fig. 11. PV1 was emulated that the short-circuit current decreased by 15%. The open voltage of the panel was designed to be 47.6 V. f_s and d were fixed at 30 kHz and 0.5, respectively. The resistance R_{out} was varied from open to short, to sweep panel characteristics.

Measured waveforms are shown in Fig. 12. The good agreement with the theoretical ones shown in Fig. 7 demonstrated the proper operation of the prototype.

The measured *P-V* characteristics of the panel with/without the proposed converter are shown in Fig. 13. Without the proposed converter, two MPPs (local and global MPPs) on the *P-V* characteristics were observed, and the maximum power was

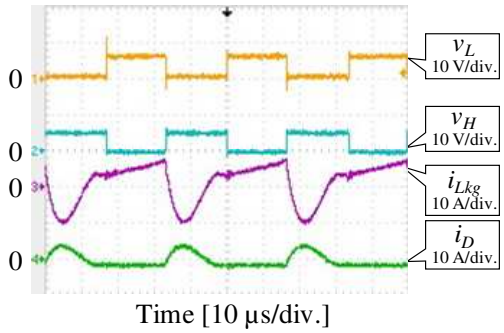

Fig. 12. Measured waveforms.

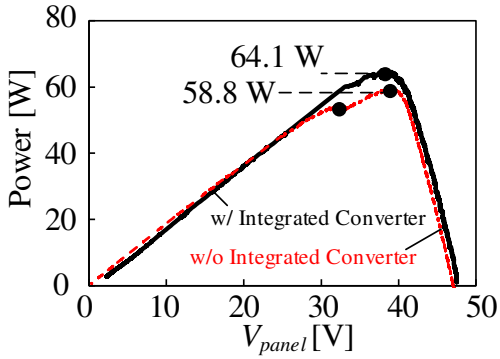

Fig. 13. *P-V* characteristics of the panel with/without proposed converter.

58.8 W. In contrast, with the proposed converter, the local MPP disappeared, and the maximum power increased to 64.1 W, improving the maximum power by 8.3%. The experimental results demonstrated that the proposed converter could prevent negative influences of the mismatch condition.

V. CONCLUSIONS

This paper proposed the integrated converter derived from the Dickson SCC and the PWM step-up converter for solar roofs of PHEVs. Integrating two converters into a single unit realizes system- and circuit-level simplifications. The proposed converter can not only automatically supply the power to the weak substrings but also achieve the arbitrary voltage step-up ratios by adjusting *N* of TI.

The experimental equalization tests using the 200-W prototype for seven substrings were performed emulating characteristic mismatch conditions. With equalization, the local MPP successfully disappeared, and the maximum power increased from 58.8 W to 64.1 W, achieving 8.3% improve in power yield. The proposed converter effectiveness was experimentally confirmed.

REFERENCES

[1] F. Wang, T. Zhu, F. Zhuo, H. Yi, and Y. Fan, "Enhanced simulated annealing-based global MPPT for different PV systems in mismatched conditions," *Journal of Power Electronics*., vol. 17, no. 5, pp. 1327–1337, Sep. 2017.

[2] M. A. Ghasemi, H. M. Forushani, and M. Parniani, "Partial shading detection and smooth maximum power point tracking of PV arrays under

PSC," *IEEE Trans. Power Electron*., vol. 31, no. 9, pp. 6281–6292, Sep. 2016.

[3] M. Gokdag and M. Akbaba, "A novel switched-capacitor topology for submodule level maximum power point tracking under partial shading and mismatch conditions," *Proc. Int. Conf. Model. Simul. Appl. Optim.*, pp. 1–5, May. 2015.

[4] G. R. Walker, and P. C. Sernia, "Cascaded DC-DC converter connection of photovoltaic modules," *IEEE Trans. Power Electron*., vol. 19, no. 4, pp. 1130–1139, Jul. 2004.

[5] G. V. Krishna and M. Tech, "Design, analysis, and implementation of solar power optimizer for DC distribution system," *IEEE Trans. Power Electron*., vol. 28, no. 4, pp. 1764–1772, Apr. 2013.

[6] M. Pisano, F. Bizzarri, and A. Brambilla, "Micro-inverter for solar power generation," *International Symposium. Power Electron. Electrical Drives. Automation and Motion. Sorrento*., pp. 109–113, 2012.

[7] S. Poshtkouhi, V. Palaniappan, M. Fard, and O. Trescases, "A general approach for quantifying the benefit of distributed power electronics for fine grained MTTP in photovoltaic applications," *IEEE Trans. Power Electron*., vol. 27, no. 11, pp. 4656–4666, Nov. 2012.

[8] H. J. Bergveld, D. Büthker. Castello, T Doorn, A. D. Jong, R. V. Otten, and K. D. Waal, "Module-level DC/DC conversion for photovoltaic systems: the delta-conversion concept," *IEEE Trans. Power Electron*., vol. 28, no. 4, pp. 2005–2013, Apr. 2013.

[9] P. S. Shenoy, K. A. Kim, B. B. Johnson, and P. T. Krein, "Differential power processing for increased energy production and reliability of photovoltaic systems," *IEEE Trans. Power Electron*., vol. 28, no. 6, pp. 2968–2979, Jun. 2013.

[10] C. Olalla, D. Clement, M. Rodriguez, and D. Maksimovic, "Architectures and control of submodule integrated DC-DC converters for photovoltaic applications," *IEEE Trans. Power Electron*., vol. 28, no. 6, pp. 2980–2997, Jun. 2013.

[11] Y. T. Jeon, H. Lee, K. A. Kim, and J. H. Park, "Least power point tracking method for photovoltaic differential power processing systems," *IEEE Trans. Power Electron*., vol. 31, no. 3, pp. 1941–1951, Mar. 2017.

[12] G. Ghu, H. Wen, L. Jiang, Y. Hu, and X. Li, "Bidirectional flyback based isolated-port submodule differential power processing for photovoltaic applications," Solar Energy, vol. 157, pp. 929–940, Oct. 2017.

[13] T. Shimizu, O. Hashimoto, and G. Kimura, "A novel high-performance utility-interactive photovoltaic inverter system," *IEEE Trans. Power Electron*., vol. 18, no. 2, pp. 704–711, Mar. 2003.

[14] M. Uno and A. Kukita, "Two-switch voltage equalizer using an LLC resonant inverter and voltage multiplier for partially shaded series-connected photovoltaic modules," *IEEE Trans. Ind. Appl*., vol. 51, no. 2, pp. 1587–1601, Mar./Apr. 2015.

[15] M. Uno and A. Kukita, "PWM converter integrating switched capacitor converter and series-resonant voltage multiplier as equalizers for photovoltaic modules and series-connected energy storage cells for exploration rovers," *IEEE Trans. Power Electron*., vol. 32, no. 11, pp. 8500–8513, Nov. 2017.

[16] M. Uno and A. Kukita, "Current sensorless equalization strategy for a single-switch voltage equalizer using multistacked buck-boost converters for photovoltaic modules under partial shading," *IEEE Trans. Ind. Appl*., vol. 53, no. 1, pp. 420–429, Jan./Feb. 2017.

[17] M. Uno and A. Kukita, "Single-switch single-magnetic PWM converter integrating voltage equalizer for partially-shaded photovoltaic modules in standalone applications," *IEEE Trans. Power Electron*., vol. 33, no. 2, pp. 1259–1270, Feb. 2018.

[18] M. Uno and T. Shinohara, "Variable switching frequency modulation scheme for PWM converter integrating series-resonant voltage multiplier-based voltage equalizer for photovoltaic strings under partial shading," *IEEJ Trans. Electrical Electronics Engineering*., vol. 14, no. 3, pp. 467–474, Mar. 2019.

[19] M. Uno and T. Shinohara, "Module-integrated converter based on cascaded quasi-Z-source inverter with differential power processing capability for photovoltaic panels under partial shading," *IEEE Trans. Power Electron*., to be published.

[20] J. T. Stauth, D. Seeman, and K. Kesarwani, "Resonant switched-capacitors for sub-module distributed photovoltaic power management," *IEEE Trans. Power Electron*., vol. 28, no. 3, pp. 1189–1198, Mar. 2013.

[21] Y. Shang, B. Xia, F. Lu, C. Zhang, N. Cui, and C. C. Mi, "A switched-coupling-capacitor equalizer for series-connected battery strings," *IEEE Trans. Power Electron*., vol. 32, no. 10, pp. 7694–7706, Oct. 2017.

[22] S. B. Yaakov, A. Blumenfeld, A. Cervera, and M. Evzelman, "Design and evaluation of a modular resonant switched capacitor equalizer for PV panels," in *Proc. IEEE Energy Convers. Congr. Expo*., 2012, pp. 4129–4136.

[23] M. Yamamoto and M Uno, "Transformerless PWM converter integrating voltage equalizer for battery and photovoltaic systems," *IEICE*, vol. 116, no. 329, pp. 5–10, Nov. 2016.